MNRAS **000**, 1–9 (2020) Preprint 13 November 2020 Compiled using MNRAS LATEX style file v3.0

Relations between the asteroseismic indices and stellar parameters of δ Scuti stars for two years of TESS Mission

A. Hasanzadeh[1]*, H. Safari[1]†,H. Ghasemi[2]

[1]*Department of Physics, Faculty of Science, University of Zanjan P.O. Box 45195-313, Zanjan, Iran*
[2]*Department of Physics, Institute for Advanced Studies in Basic Sciences (IASBS), Zanjan 45137-66731, Iran*

Accepted XXX. Received YYY; in original form ZZZ

ABSTRACT

We aim to study the relationship between the asteroseismic indices and the physical quantities of δ Scuti stars observed by the TESS mission at 26 sectors. For 561 δ Scuti targets the asteroseismic indices such as fundamental frequency, large frequency separation ($\Delta\nu$), frequency of the highest peak in the spectrum, the peak of the envelope of oscillation mode ($\nu_{\rm max}$), and stellar physical parameters (effective temperature, surface gravity, density, etc.), the scaling relations are investigated. We modified the relation between the large frequency separation and mean stellar density (ρ) as $\Delta\nu = 0.79\rho^{0.42}$. About one-third of our δ Scuti cases showed a highly positive correlation between the fundamental radial pressure mode and the large frequency separation, which these cases can be satisfied the established relation of the period and luminosity. We obtained a scaling the relation between the large frequency separation and $\nu_{\rm max}$ as $\Delta\nu = 1.99\nu_{\rm max}^{0.70}$ which is close to that of a solar-like and red giant stars. We showed that $\nu_{\rm max}$ has a strong positive correlation with the effective temperature; however, a very strong positive correlation is obtained between $\nu_{\rm max}$ and the effective temperature multiplying by the surface gravity of stars.

Key words: asteroseismology – techniques: photometric: TESS stars: variables: δ Scuti

1 INTRODUCTION

Asteroseismology is a useful task to diagnose the internal and physical structure of pulsating stars via the interpretation of the normal mode spectrum (Brown & Gilliland 1994; Dupret et al. 2004b; Aerts et al. 2010; Catelan & Smith 2015; García & Ballot 2019). Due to high-resolution data received by recent several space missions such as MOST (Walker et al. 2003), CoRoT (Auvergne et al. 2009), Kepler (Koch et al. 2010; Gilliland et al. 2010) the asteroseismology methods have been considerably developed (**?**Hon et al. 2019). Recently, NASA's mission Transiting Exoplanet Survey Satellite (TESS) provides high-quality photometric light curves nearby stars for asteroseismic analysis (Campante et al. 2016). TESS surveys the most (about 85 percent) sky within the 26 sectors during two years of the primary mission (Ricker et al. 2015).

In the Hertzsprung-Russell (HR) diagram δ Scuti stars with the masses between 1.5 and 2.5$M_\odot$ are classified in the category of variable stars (Breger 2000a; Antoci et al. 2019). They mostly show low-order p modes with frequencies in the range 5–80 cycle per day (1/d), which may be excited by the κ mechanism operating in the He II partial ionization region (Breger 2000b; Dupret et al. 2004a; Balona 2014; Xiong et al. 2016). The effective temperature of δ Scuti stars is in the range of 6000 to 9000 Kelvin, which classified as late A- and early F-type stars (Uytterhoeven et al. 2011). Some of the δ Scuti stars show the gravity (g) modes in their spectrum, which may be classified as hybrid stars (Balona & Dziembowski 2011; Bradley et al. 2015). Based on the Kepler light curves Bowman & Kurtz (2018) showed that about 25 percent of the δ Scuti stars are hybrid variables. The hybrid oscillating stars represent both p and g- modes, which allow us to study the stellar envelopes and cores (Grigahcène et al. 2010).

Scaling relations investigate the asteroseismic indices and global stellar parameters to estimate the stellar fundamental parameters for the structure and evolution (Coelho et al. 2015; Hekker 2020; Brown et al. 1991). Examining the scaling relations' validity between the asteroseismic and stellar parameters is very important in asteroseismology (Bellinger 2019). Theoretical modeling showed that the large frequency separation is closely related to the mean stellar density's square root (Aerts et al. 2010; Kjeldsen & Bedding 1995). So, measuring the large frequency separation with considerable accuracy is critical in the asteroseismic analysis of pulsating stars. Usually, the mean large frequency separation between the consecutive frequency of radial modes and the frequency of maximum oscillating power can be used to estimate the stellar parameters such as mass and radius (Kallinger et al. 2010b; Mosser

* E-mail: hasanzadeh@znu.ac.ir † E-mail: safari@znu.ac.ir

et al. 2010; Kallinger et al. 2010a). Suárez et al. (2014) found that the mean large frequency separation is related to the mean stellar density of the δ Scuti stars. García Hernández et al. (2015, 2017) used the characteristics of eclipsing binaries with a δ Scuti component to determine the relationship between the mean stellar density and large frequency separation, which was slightly departed from the theoretical relation. Bedding et al. (2020) modified the theoretical relation for the mean large separation of 60 δ Scuti stars observed by TESS, which approximately equals to 0.85 of the theoretical value. Furthermore, Stello et al. (2009) showed the large frequency separation is related to the maximum power frequency for solar-like stars. The relation between the effective temperature and frequencies of star is another critical issue in asteroseismology (Barceló Forteza et al. 2020). Balona & Dziembowski (2011) showed that the effective temperature of δ Scuti stars are positively correlated with the mode's frequency with the highest-peak amplitude.

Here, we used the TESS data to study the asteroseismic properties of 561 δ Scuti candidates. To do this, we apply several frequency analysis packages to obtain the frequency of oscillations of stars. Also, we collect the stellar parameters of these stars from the latest TESS catalogue. The relation between the asteroseismic indices and stellar parameters is investigated.

This paper is organized as follows: Section 2 gives the data for δ Scuti stars. Section 3 introduces the light curve and asteroseismic analysis. Sections 4 and 5 represent the results and conclusion, respectively.

2 DATA

The Transiting Exoplanet Survey Satellite (TESS) is a NASA mission launched in April 2018. TESS is a high-precision photometric instrument and developed to monitor stars to find exoplanets via transit methods (Sullivan et al. 2015; Barclay et al. 2018). Characterization of stars through asteroseismology allows determining the properties of their interiors (Huber et al. 2013; Silva Aguirre et al. 2015).

TESS primary mission probed the sky in 26 sectors for more than several million stars in a red filter of approximately 600-1000 nm (Silva Aguirre et al. 2015). TESS observed each sector for 27 days (Barclay et al. 2018). Around 200,000 stars with a cadence of 2 minutes were observed to determine stellar parameters via asteroseismology methods (Stassun et al. 2018; Feinstein et al. 2019; Campante et al. 2016). TESS data is collected from the Mikulski Archive for Space Telescopes (MAST)[1] in both target pixel files (TPF) and light curves (LC) files. The LC is recorded in Simple Aperture Photometry (SAP) and calibrated Pre-search Data Conditioning Simple Aperture Photometry (PDCSAP). See (Jenkins et al. 2016), for more details. Here, we analysed the short cadence (2 min) PDCSAP light curve of 561 δ Scuti stars for two years of observation in sectors 1 to 26. The position of these stars in the celestial sphere is shown in Fig. 1. We selected targets mainly from TESS Asteroseismic Science Consortium (TASC)-WG4(AF-stars)[2] list. We also checked the list of δ Scuti stars with Kepler's mission (Bradley et al. 2015; Uytterhoeven et al. 2011). Our goal is to analyse the δ Scuti stars with a large number of frequencies, so we limited our list by removing the high amplitude δ Scuti (HADS) and SX Phe stars with single or double modes. To create statistical and scaling

[1] https://archive.stsci.edu [2] https://tasoc.dk/wg4

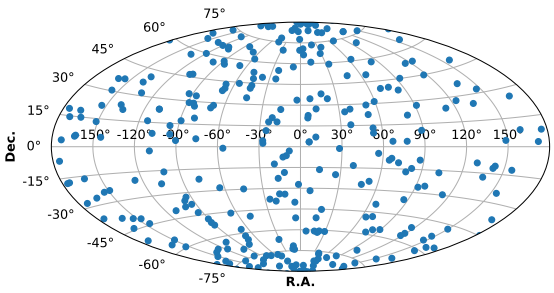

Figure 1. Position (RA and Dec) of 561 δ Scuti stars (blue dots) in the celestial sphere were detected from July 2018 to July 2020 by TESS mission

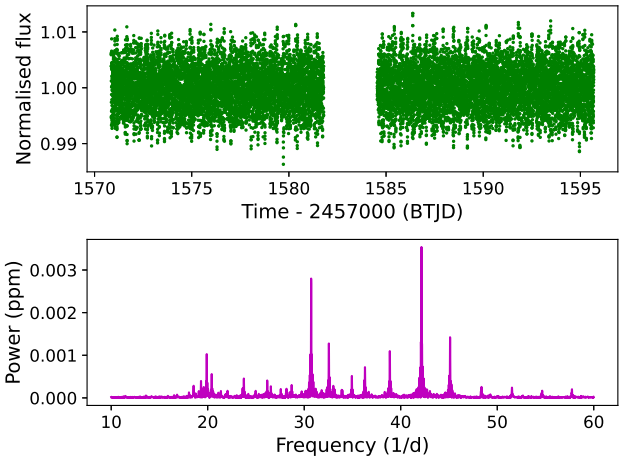

Figure 2. Upper panel: Normalised flux (light curve) of a δ Scuti star TIC9591460 recorded by TESS during sector 10. Lower panel: The Lomb–Scargle periodogram represents amplitudes (in ppm units) versus the frequencies (cycle per day)

relations for a list of δ Scuti stars, we used the latest TESS catalogue (Stassun et al. 2019). The positions (in right ascension and declination coordinate), magnitudes in different filters (B, V, Gaia, TESS), and stellar parameters (effective temperature, mass, radius, surface gravity, metallicity) are extracted from the TESS catalogue.

3 METHODS

3.1 Light curve analysis

The frequency modes of 561 selected δ Scuti stars were analysed. To do this, first, 4σ outlier data points were removed from the PDCSAP light curves of each star. Then, the resultant light curves are normalised to their average intensity and smoothed by a second-order Savitzky-Golay filter (Savitzky & Golay 1964). A sample light curve for TIC9591460 is represented in Fig. 2. changing the size of aperture pixel files for each star (Fig. 3) is a standard way to increase the analysis accuracy. For too small aperture pixel file, increasing the aperture size for a target allows capturing extra flux. Also, de-

creasing the size of the aperture may remove the contamination effects from nearby objects and increase the SNR (Lund et al. 2017; Marchiori et al. 2019). We extracted the light curve for each case from TPFs to compare with the PDCSAP light curve and improve the periodogram's signal-to-noise. A standard Lomb-Scargle periodogram via the LightKurve package (Lightkurve Collaboration et al. 2018) was applied to the light curves to extract the frequency of oscillations. Lightkurve is an open-source package to extract the photometric data for TESS observations. This package provides the asteroseismic power spectra and oscillation modes. In the analysis, the frequencies with the significant signal-to-noise ratio were considered. To ensure the validity of frequencies, we also applied other standard frequency analysis codes (KU Leuven pipeline: (Degroote et al. 2009); SMURFS: (Müllner 2020)). The KU Leuven iterative pre-whitening pipeline uses the Lomb-Scargle periodogram and multi-frequency non-linear least-squares optimization method to find the frequencies and their amplitudes (Pápics et al. 2012; Van Reeth et al. 2015). SMURFS developed to obtain frequencies of light curves from TESS observations. This code can compute the possible frequency combinations instead of the pre-whitening method.

3.2 Asteroseismic analysis

In asteroseismology, a star's basic information can be deduced from the seismic indices. The relations between the global seismic indices (frequency of the highest-peak amplitude, fundamental frequency, large frequency separation, etc.) and stellar characteristics (mass, gravity, temperature, radius, etc.) have been widely developed (Coelho et al. 2015; Yu et al. 2018; Barceló Forteza et al. 2020). Oscillations of a star are interpreted via a superposition of the radial wave function and spherical harmonics. Each mode indicates with the radial order (n), the spherical degree (l), and the azimuths order (m), which represent the properties of the oscillations. The fundamental radial mode defines with the radial order $n = 1$ and spherical number $l = 0$ that is expected to be appear with a highest-peak amplitude in the power spectrum. However, the previous study (Bedding et al. 2020) on the δ Scuti stars' pulsations showed that the fundamental radial modes did not show the highest-peak amplitudes in the spectrum. In our analysis, the smallest frequency in the power spectrum with the amplitude at least greater than 0.2 of the highest-peak amplitude is chosen as the fundamental radial mode of the pulsating scuti star (Fig. 4). Studies (Breger & Bregman 1975; McNamara 2011) showed that the δ Scuti stars follow a relation between the pulsation period (P) and the luminosity. Ziaali et al. (2019) obtained the period-luminosity relation as $M_V = (-2.94 \pm 0.06) \log P(\text{day}) - (1.34 \pm 0.06)$ in which M_V is the absolute visible magnitude. Our results show that about one-third of fundamental modes obey this relation, which is in good agreement with the previous study (Bedding et al. 2020). For the power spectrum of each δ Scuti star, the frequency related to the highest-peak amplitude is called NuMaximum. It is well-known that due to amplitude modulation mechanisms and noise background, the NuMaximum may change with time. Therefore, it was suggested to use the frequency (ν_{max}) of the peak of the envelope for oscillation modes in a signal-to-noise ratio (SNR) periodogram instead of the NuMaximum. The SNR periodogram is generated by dividing the power by the noise spectrum. Applying an autocorrelation method (Barceló Forteza et al. 2020) the frequency ν_{max} is determined (Fig. 5). Viani et al. (2019) gives the details of the method to determine the $\nu_{\max}$.

Large frequency separation ($\Delta\nu$) is another important seismic

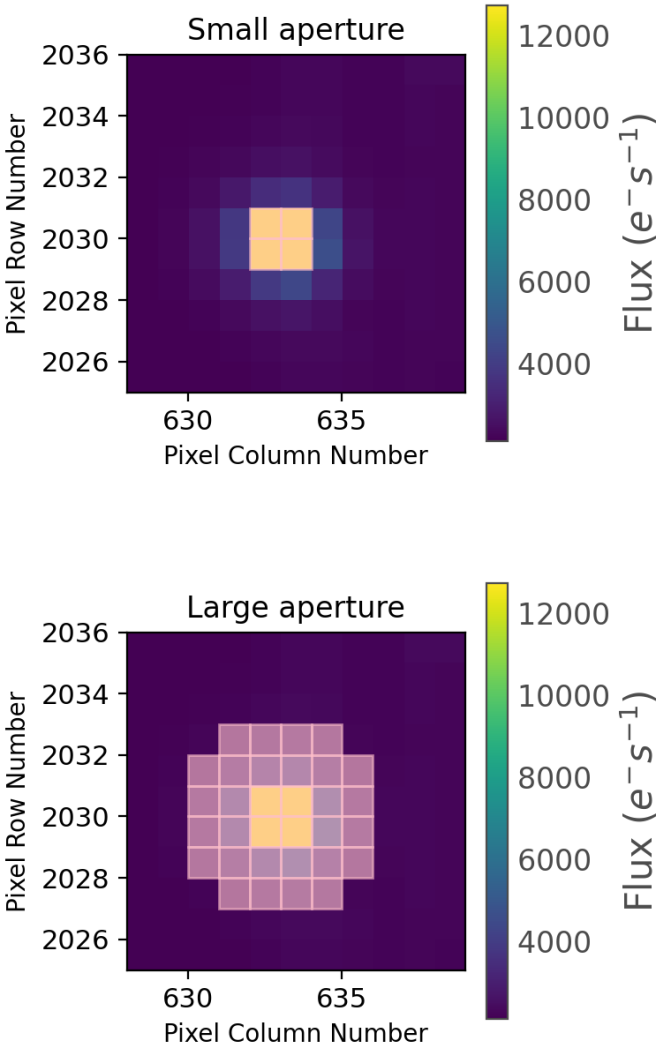

Figure 3. Pixel file image of TIC9591460 star for the small (left) and large (right) apertures (mask).

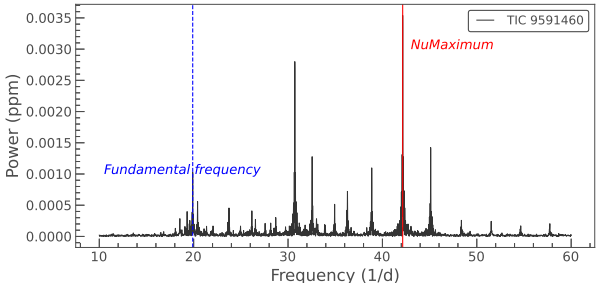

Figure 4. Fundamental frequency (dashed blue line) and NuMaximum (red line) for TIC9591460.

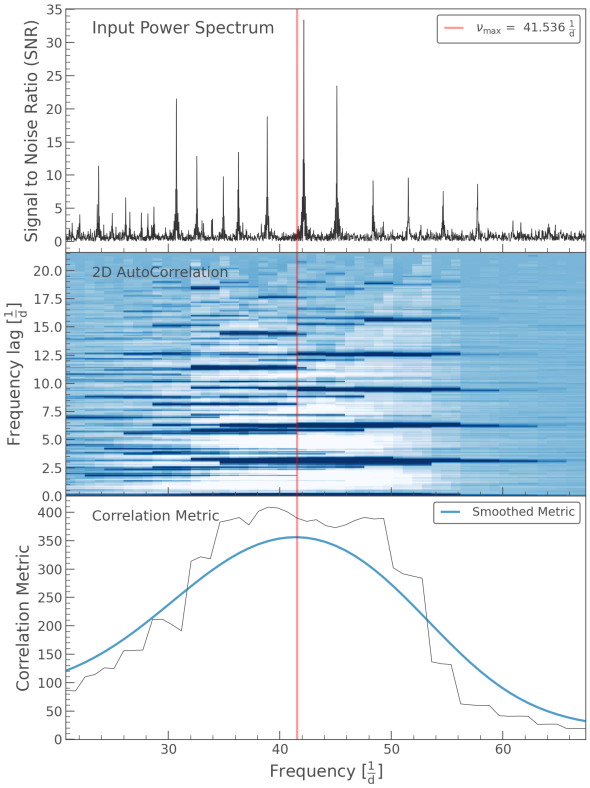

Figure 5. Upper panel: The SNR periodogram for TIC9591460. The red line indicates the ν_{max}. Middle panel: Two-dimensional autocorrelation applied to periodogram. Lower panel: The mean collapsed correlation versus central frequency (see Viani et al. (2019)), and a Gaussian smoothing curve is presented in blue.

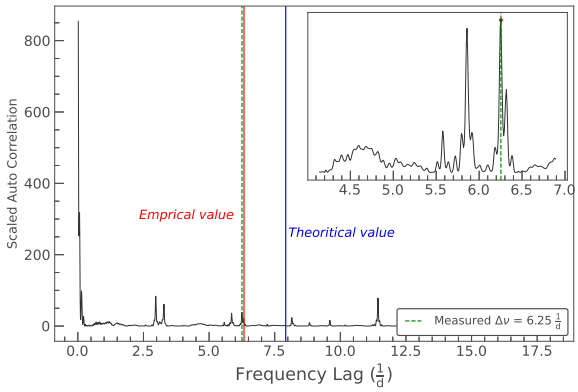

Figure 6. The large frequency separation ($\Delta\nu$) of the seismic oscillations of TIC9591460 using an 2D autocorrelation method. The theoretical ($\Delta = \sqrt{\rho}$), empirical ($\Delta\nu = 0.78\rho^{0.46}$), and calculated based on the 2D autocorrelation method for the large frequency separation are indicated by blue, red, and dashed green lines, respectively.

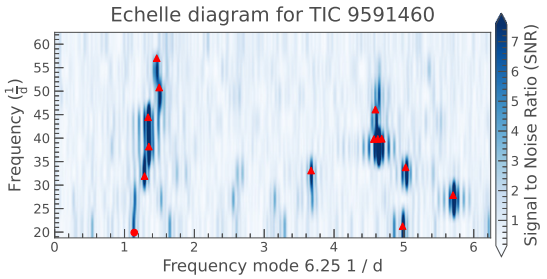

Figure 7. The echelle diagram in a colour scale for TIC9591460 with an average large frequency separation about $\Delta\nu$=6.25 1/d. The circle and triangles indicate the fundamental mode and high overtone modes, respectively.

quantity. For an angular degree (l), $\Delta\nu$ defines the average frequency spacing between modes of neighbouring on radial order (n) (Aerts et al. 2010). For a given ν_{max}, a window with the size of one full-width-half-maximum of the mode envelope (includes all of the visible mode peaks) is considered on both sides. Then, an 2D autocorrelation method is applied to the regions around the ν_{max}. Details of the 2D autocorrelation method was given by (Viani et al. 2019). Using an automatic peak finding algorithm for the peaks in the vicinity of an empirical value (will be discussed later) is chosen as the final value for the large frequency separation (see Fig. 6) (Huber et al. 2009; Mosser & Appourchaux 2009). The empirical relations between the mean density (ρ) and $\Delta\nu$ for δ Scuti stars were investigated (García Hernández et al. 2015; Chen et al. 2019). In the literature, for oscillation modes with $n \gg l$, a theoretical asymptotic relation between the large frequency separation and mean stellar density was investigated as $\Delta\nu = \sqrt{\rho}$ (Aerts et al. 2010; Tassoul 1980; Ulrich 1986; Kjeldsen et al. 1995). It was accepted that the mode spacing of stars seems to be not fully regular, so it expected that $\Delta\nu$ varies with the frequencies (Paparó et al. 2016; Mirouh et al. 2019). Suárez et al. (2014) predicted an empirical scaling relations between the large frequency separation and mean stellar density as $\Delta\nu = 0.78\rho^{0.46}$. Also, based on the TESS and Kepler observations for 60 δ Scuti stars (Bedding et al. 2020) a modified relation was obtained as ($\Delta\nu = 0.85\sqrt{\rho}$). This relation holds between the theoretical asymptotic relation and the empirical scaling relation (See Fig. 12). In our analysis, the large frequency separation of the δ Scuti stars within the range of theoretical and empirical scaling relation is considered for statistical study. Finally, we used the echelle diagram (Grec et al. 1983) to confirm the large frequency separations for δ Scuti stars. An echelle diagram is a useful tool in asteroseismology to display the oscillation frequencies and helps us to mode identification. The frequency spectrum is divided into segments of $\Delta\nu$ and collects them in a diagram to make an echelle diagram. In the diagram, the modes with a similar angular degree are arranged close to a vertical ridge. The considerable variations in the large frequency separation have appeared like curvature in the diagram. As expected, close to the vertical ridges have corresponded to the correct $\Delta\nu$ in the diagram (Fig. 7).

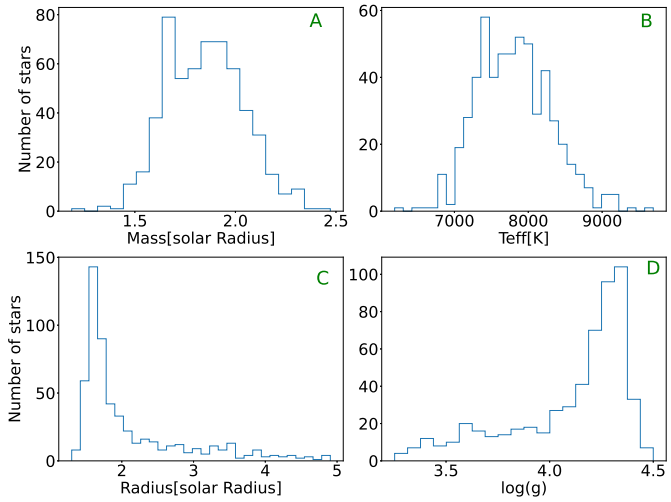

Figure 8. Frequency distribution of the mass (A), radius (B), effective temperature (C), and surface gravity (D) for 561 δ Scuti stars.

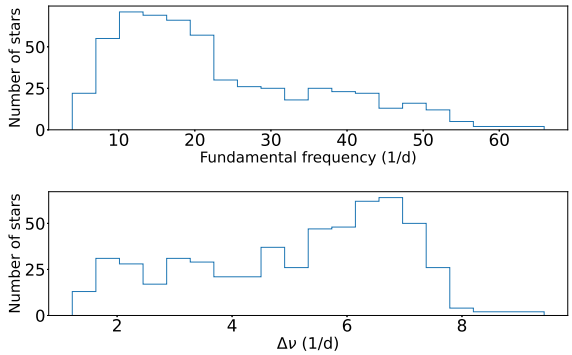

Figure 9. Frequency distribution of the fundamental frequency (c/day) and large separation (c/day) for 561 δ Scuti stars.

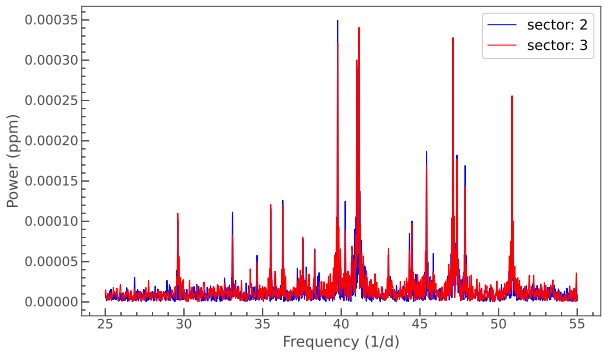

Figure 10. Frequency power spectrum of TIC66434034 star observed in sector 2 (blue line) and 3 (red line). The frequency with highest peak (asterisk) and amplitude of other frequencies are changed with time.

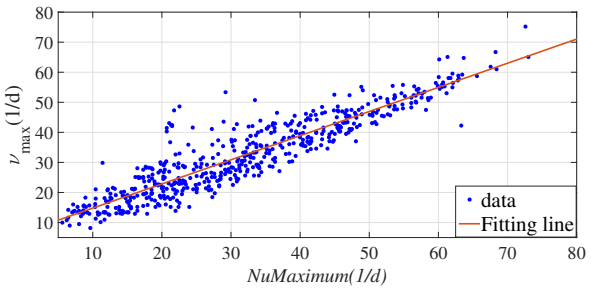

Figure 11. Scatter plot of NuMaximum versus $\nu_{\rm max}$. The NuMaximum is highly correlated (Pearson correlation about 0.92) with $\nu_{\rm max}$.

4 RESULTS

For 561 δ Scuti stars observed with the TESS mission, the asteroseismic quantities are determined. Positions (in right ascension and delineation) of stars in the celestial sphere are distributed in different sectors (Fig. 1). The stellar parameters for these stars are extracted from the revised TESS input catalogue (Stassun et al. 2019).

The statistical analysis and scaling relations are studied. Fig. 8 represents the frequency distribution of mass, radius, effective temperature, and surface gravity for 561 Scuti stars. As shown in the figure, the mass, radius, effective temperature, and surface gravity for Scuti stars are in the range of 1.2 to 2.5$M_{\odot}$, 1.3 to 4.9$R_{\odot}$, 6200 to 9700 K, and 3.3 to 4.5, respectively. Mass and effective temperature value agree with the previous reports for δ Scuti stars (Daszyńska-Daszkiewicz 2007; Antoci et al. 2019). In Table 1 the asteroseismic indices and stellar parameters for a sample of 50 δ Scuti stars are presented. A supplement to this paper provides the electronic table contains the sector number, positions, asteroseismic indices, and stellar quantities for 561 δ Scuti stars.

Fig. 9 shows the histogram (frequency-size distribution) of the fundamental frequency and large frequency separation for 561 Scuti stars. The fundamental frequency and large frequency separation are changed in the range of 3.9 to 65.9 1/d and 1.22 to 9.43 1/d, respectively. The peak of distribution for the fundamental frequency is about 15 1/d.

The scatter plot of NuMaximum via $\nu_{\rm max}$ is shown in Fig. 11. We see that NuMaximum is highly correlated (correlation coefficient r=0.92) with $\nu_{\rm max}$ for δ Scuti stars. Also, the frequency with highest-peak amplitude may change with time (Fig. 10), so we used ν_{max} instead of mode with the highest-peak amplitude in our further analysis. Figure 12 depicts the relation between the large frequency separation and mean stellar density for δ Scuti stars. A power function $\Delta\nu = (0.788 \pm 0.013)\rho^{(0.423\pm0.016)}$ is fitted. As we see in the figure, the fitted relation is slightly changed from the theoretical and predicted relations (Suárez et al. 2014; Bedding et al. 2020).

The relation between the $\nu_{\rm max}$ and effective temperature of 561 targets is shown in Fig. 13. We see a strong positive correlation (correlation coefficient r=0.65) between the $\nu_{\rm max}$ and $T_{\rm eff}$ which is recognized with the surface gravity in the colour plot (Fig. 13 upper panel). But, the effective temperature multiplying by the surface gravity ($gT_{\rm eff}$) shows a very strong positive correlation (r=0.83) with $\nu_{\rm max}$ (Fig. 13 lower panel).

Figure 14 illustrates the relation between the fundamental frequency (ν_f) and the large frequency separation for the Scuti stars. About one-third (34 percent) of stars (green asterisks in the fig-

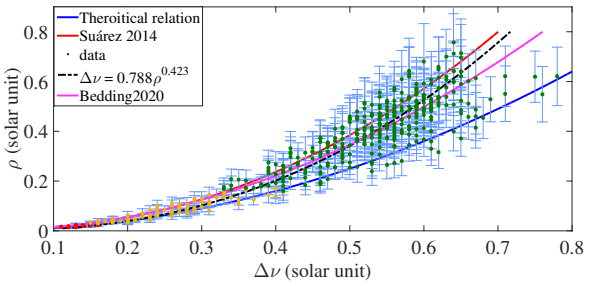

Figure 12. The mean stellar density (ρ) versus the large frequency separation ($\Delta\nu$) for 561 δ Scuti stars which recognised with $3 \leqslant \log g \leqslant 3.5$ (red circles) , $3.5 < \log g \leqslant 4.0$ (yellow circles), and $4.0 < \log g \leqslant 4.5$ (green circles). The fitted curve $\Delta\nu = (0.79 \pm 0.01)\rho^{0.42\pm0.02}$ is represented by dotted black line. The theoretical relation (blue line) $\Delta\nu = \sqrt{\rho}$ (Aerts et al. 2010), the empirical relations $\Delta\nu = 0.78\rho^{0.46}$ (red line) and $\Delta\nu = 0.85\sqrt{\rho}$ (purple line) are given by Suárez et al. (2014) and Bedding et al. (2020), respectively.

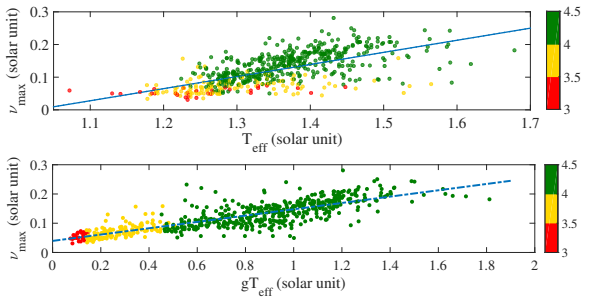

Figure 13. Upper panel: Relation between the $\nu_{\max}$ and effective temperature. The correlation coefficient is obtained about r=0.65. Lower panel: Relation between the $\nu_{\max}$ and effective temperature multiplying by surface gravity ($gT_{\rm eff}$). The correlation coefficient is obtained about r=0.83. The δ Scuti stars classify in three groups with different surface gravity as explained in Figure 12.

ure) obey the well-known relationship between the period and observed luminosity. The fundamental frequency and the large frequency separation for these stars satisfy a positive correlation as $\nu_f = (2.63 \pm 0.24)\Delta\nu + (2.66 \pm 1.24)$. A power relation between the large frequency separation and $\nu_{\max}$ for δ Scuti stars is obtained as $\Delta\nu = (1.99 \pm 0.16)\nu_{\max}^{(0.70\pm0.04)}$ (Fig. 15). Previous studies (Stello et al. 2009; Huber et al. 2011; Yu et al. 2018) showed that $\Delta\nu$ is related to $\nu_{\max}$ with a power function with exponent in the range of 0.7 to 0.8 for the solar like and red giant stars. The stars classify in three groups with different surface gravity $3 \leqslant \log g \leqslant 3.5$, $3.5 < \log g \leqslant 4.0$, and $4.0 < \log g \leqslant 4.5$, which is related to the zero-age main sequence (ZAMS), Mid-age main sequence (MAMS), and Terminal-age main sequence (TAMS) stars, respectively (Bowman & Kurtz 2018).

5 CONCLUSION

We applied the frequency analysis to find the asteroseismic indices of 561 δ Scuti stars observed during two years of TESS mission. Our samples' largest frequency limit is obtained about 80 1/d,

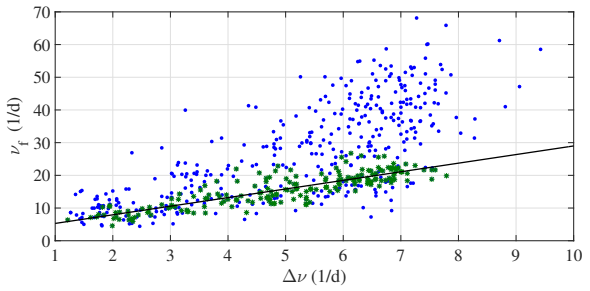

Figure 14. Scatter plot of the large frequency separation (1/d) versus the fundamental frequency (1/d). The colour of each target represents its related surface gravitation.

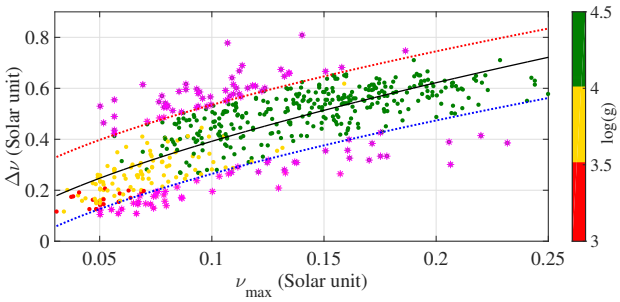

Figure 15. Scatter plot for the large frequency separation and $\nu_{\max}$ for 561 δ Scuti stars. The power curve (black line) $\Delta\nu = a\nu_{\max}^{b}$ with a =1.99±0.16 and b =0.70±0.04 is fitted to values indicated with green, yellow, and red colours. The values outside of two dashed lines (purple colour) were not considered in the fitting analysis. The auxiliary information is given at Figure 12.

which verifies the previous observations (Breger 2000b; Bowman & Kurtz 2018). The stellar parameters of the stars were collected from the latest TESS catalogue. Statistical analysis shows that their mass,effective temperature, and surface gravity of δ Scuti samples are in the range of 1.2 to 2.5$M_{\odot}$, 6200 to 9700 K, and 3.3 to 4.5, respectively.

The main results of this paper are summarised as follows:

- For our samples, the fundamental frequencies ν_f was obtained in the range of 3.9 to 65.9 1/d. For 19 percent of samples, the fundamental frequencies have corresponded to the highest-peak amplitudes of the power spectrum, but for the remaining stars, ν_f was not to have the highest peak of the power spectrum. It seems the peak value of amplitudes is sensitive to the line of sight (point of view) of the observer or instrument (Lignières & Georgeot 2009). Also, as we observed in the power spectrum for sectors 2 and 3 for TIC66434034 star (Fig. 10), the frequency with the highest power is not fixed with time (Handler et al. 1998; Breger 2000b; Barceló Forteza et al. 2015). Another reason for changing the highest amplitude of frequency may be related to the long-term variability behaviour, and frequency or phase modulation of many of δ Scuti stars (Bowman et al. 2016; Khalack et al. 2019). Numerical modeling via the stellar oscillation codes (e.g., GYRE) may accurately address the physical mechanisms behind the amplitude variation of frequency on δ Scuti stars.
- We find that the fundamental frequency (the smallest frequency

with the the highest-peak amplitude or without the highest-peak amplitude) of 33 percent of cases satisfy the period-luminosity relation. Bedding et al. (2020) identified one-third of samples that the highest peak with the frequency in the range of 18 to 23 1/d are corresponded to the fundamental mode and agree with the empirical period-luminosity relation. For these stars, We found a linear relation as $\nu_f = (2.63 \pm 0.24)\Delta\nu + (2.66 \pm 1.24)$ for the fundamental frequency and the large frequency separation, which is in agreement with (Bedding et al. 2020).

- We obtained a relation between the large frequency separation and mean stellar density as $\Delta\nu = (0.79 \pm 0.01)\rho^{0.42\pm0.02}$ for δ Scuti stars (Fig. 12) which is slightly differ from the theoretical and empirical relations (Suárez et al. 2014; Bedding et al. 2020). This asteroseismic relation can help us to determine the mean stellar density of individual δ Scuti stars with analysing the photometric light curves (Huber et al. 2019).

- We obtained a positive correlation between the $\Delta\nu$ and $\nu_{\rm max}$ as $\Delta\nu$ and $\nu_{\rm max}$ as $\Delta\nu = (1.99 \pm 0.16)\nu_{\rm max}^{(0.70\pm0.04)}$ (Fig. 15) for Scuti stars. In this analysis, we see that the stars are classified in three groups with surface gravity $3 \leqslant \log g \leqslant 3.5$, $3.5 < \log g \leqslant 4.0$, and $4.0 < \log g \leqslant 4.5$, which is related to the ZAMS, MAMS, and TAMS stars, respectively. This classification of Scuti stars in different groups via the surface gravity can be considered an indicator in their evolutionary stages (Bowman & Kurtz 2018; Barceló Forteza et al. 2020).

- We obtained a strong positive correlation (Pearson=0.65) between the peak of the envelope of oscillation modes and effective temperature of 561 targets (Fig. 13) which is in good agreement with (Breger 2000b; Bowman & Kurtz 2018; Barceló Forteza et al. 2020). However, we found a very strong positive correlation (Pearson=0.83) between the peak of the the envelope of oscillation modes and the effective temperature multiplying by surface gravity ($gT_{\rm eff}$) of stars.

ACKNOWLEDGMENTS

This manuscript includes data collected by the TESS mission, which are publicly available from the Mikulski Archive for Space Telescopes (MAST). Funding for the TESS mission is provided by the NASA Explorer Program. Funding for the TESS Asteroseismic Science Operations Centre is provided by the Danish National Research Foundation (Grant agreement no.: DNRF106), ESA PRODEX (PEA 4000119301) and Stellar Astrophysics Centre (SAC) at Aarhus University.

REFERENCES

Aerts C., Christensen-Dalsgaard J., Kurtz D. W., 2010, Asteroseismology
Antoci V., et al., 2019, MNRAS, 490, 4040
Auvergne M., et al., 2009, A&A, 506, 411
Balona L. A., 2014, MNRAS, 437, 1476
Balona L. A., Dziembowski W. A., 2011, MNRAS, 417, 591
Barceló Forteza S., Michel E., Roca Cortés T., García R. A., 2015, A&A, 579, A133
Barceló Forteza S., Moya A., Barrado D., Solano E., Martín-Ruiz S., Suárez J. C., García Hernández A., 2020, A&A, 638, A59
Barclay T., Pepper J., Quintana E. V., 2018, ApJS, 239, 2
Bedding T. R., et al., 2020, Nature, 581, 147
Bellinger E. P., 2019, MNRAS, 486, 4612
Bowman D. M., Kurtz D. W., 2018, MNRAS, 476, 3169
Bowman D. M., Kurtz D. W., Breger M., Murphy S. J., Holdsworth D. L., 2016, MNRAS, 460, 1970
Bradley P. A., Guzik J. A., Miles L. F., Uytterhoeven K., Jackiewicz J., Kinemuchi K., 2015, AJ, 149, 68
Breger M., 2000a, in Breger M., Montgomery M., eds, Astronomical Society of the Pacific Conference Series Vol. 210, Delta Scuti and Related Stars. p. 3
Breger M., 2000b, MNRAS, 313, 129
Breger M., Bregman J. N., 1975, ApJ, 200, 343
Brown T. M., Gilliland R. L., 1994, ARA&A, 32, 37
Brown T. M., Gilliland R. L., Noyes R. W., Ramsey L. W., 1991, ApJ, 368, 599
Campante T. L., et al., 2016, ApJ, 830, 138
Catelan M., Smith H. A., 2015, Pulsating Stars
Chen X., Li Y., Zhang X., 2019, ApJ, 887, 253
Coelho H. R., Chaplin W. J., Basu S., Serenelli A., Miglio A., Reese D. R., 2015, MNRAS, 451, 3011
Daszyńska-Daszkiewicz J., 2007, Communications in Asteroseismology, 150, 32
Degroote P., et al., 2009, A&A, 506, 111
Dupret M. A., Grigahcène A., Garrido R., Gabriel M., Scuflaire R., 2004a, A&A, 414, L17
Dupret M. A., Thoul A., Scuflaire R., Daszyńska-Daszkiewicz J., Aerts C., Bourge P. O., Waelkens C., Noels A., 2004b, A&A, 415, 251
Feinstein A. D., et al., 2019, PASP, 131, 094502
García R. A., Ballot J., 2019, Living Reviews in Solar Physics, 16, 4
García Hernández A., Martín-Ruiz S., Monteiro M. J. P. F. G., Suárez J. C., Reese D. R., Pascual-Granado J., Garrido R., 2015, ApJ, 811, L29
García Hernández A., et al., 2017, MNRAS, 471, L140
Gilliland R. L., et al., 2010, PASP, 122, 131
Grec G., Fossat E., Pomerantz M. A., 1983, Sol. Phys., 82, 55
Grigahcène A., et al., 2010, ApJ, 713, L192
Handler G., Pamyatnykh A. A., Zima W., Sullivan D. J., Audard N., Nitta A., 1998, MNRAS, 295, 377
Hekker S., 2020, Frontiers in Astronomy and Space Sciences, 7, 3
Hon M., Stello D., García R. A., Mathur S., Sharma S., Colman I. L., Bugnet L., 2019, MNRAS, 485, 5616
Huber D., Stello D., Bedding T. R., Chaplin W. J., Arentoft T., Quirion P. O., Kjeldsen H., 2009, Communications in Asteroseismology, 160, 74
Huber D., et al., 2011, ApJ, 743, 143
Huber D., et al., 2013, ApJ, 767, 127
Huber D., et al., 2019, AJ, 157, 245
Jenkins J. M., et al., 2016, in Software and Cyberinfrastructure for Astronomy IV. p. 99133E, doi:10.1117/12.2233418
Kallinger T., et al., 2010a, A&A, 509, A77
Kallinger T., et al., 2010b, A&A, 522, A1
Khalack V., et al., 2019, MNRAS, 490, 2102
Kjeldsen H., Bedding T. R., 1995, A&A, 293, 87
Kjeldsen H., Bedding T. R., Viskum M., Frand sen S., 1995, AJ, 109, 1313
Koch D. G., et al., 2010, ApJ, 713, L79
Lightkurve Collaboration et al., 2018, Lightkurve: Kepler and TESS time series analysis in Python (ascl:1812.013)
Lignières F., Georgeot B., 2009, A&A, 500, 1173
Lund M. N., Handberg R., Kjeldsen H., Chaplin W. J., Christensen-Dalsgaard J., 2017, in European Physical Journal Web of Conferences. p. 01005 (arXiv:1610.02702), doi:10.1051/epjconf/201716001005
Marchiori V., et al., 2019, A&A, 627, A71
McNamara D. H., 2011, AJ, 142, 110
Mirouh G. M., Angelou G. C., Reese D. R., Costa G., 2019, MNRAS, 483, L28
Mosser B., Appourchaux T., 2009, A&A, 508, 877
Mosser B., et al., 2010, A&A, 517, A22
Müllner M., 2020, SMURFS: Automated frequency extraction from time series data, doi:10.5281/zenodo.3635801, https://doi.org/10.5281/zenodo.3635801
Paparó M., Benkő J. M., Hareter M., Guzik J. A., 2016, ApJS, 224, 41
Pápics P. I., et al., 2012, A&A, 542, A55
Ricker G. R., et al., 2015, Journal of Astronomical Telescopes, Instruments, and Systems, 1, 014003
Savitzky A., Golay M. J. E., 1964, Analytical Chemistry, 36, 1627

Silva Aguirre V., et al., 2015, MNRAS, 452, 2127
Stassun K. G., et al., 2018, AJ, 156, 102
Stassun K. G., et al., 2019, AJ, 158, 138
Stello D., Chaplin W. J., Basu S., Elsworth Y., Bedding T. R., 2009, MNRAS, 400, L80
Suárez J. C., García Hernández A., Moya A., Rodrigo C., Solano E., Garrido R., Rodón J. R., 2014, A&A, 563, A7
Sullivan P. W., et al., 2015, ApJ, 809, 77
Tassoul M., 1980, ApJS, 43, 469
Ulrich R. K., 1986, ApJ, 306, L37
Uytterhoeven K., et al., 2011, A&A, 534, A125
Van Reeth T., et al., 2015, A&A, 574, A17
Viani L. S., Basu S., Corsaro E., Ball W. H., Chaplin W. J., 2019, ApJ, 879, 33
Walker G., et al., 2003, PASP, 115, 1023
Xiong D. R., Deng L., Zhang C., Wang K., 2016, MNRAS, 457, 3163
Yu J., Huber D., Bedding T. R., Stello D., Hon M., Murphy S. J., Khanna S., 2018, ApJS, 236, 42
Ziaali E., Bedding T. R., Murphy S. J., Van Reeth T., Hey D. R., 2019, MNRAS, 486, 4348

Table 1. TIC number, Sector number, positions (in RA and Dec), Effective temperature ($T_{\rm eff}$), mass ($M/M_{\odot}$), radius ($R/R_{\odot}$), surface gravity ($\log g$), luminosity ($L/L_{\odot}$), Density ($\rho/\rho_{\odot}$),TESS magnitude, fundamental frequency (ν_f), the highest-peak of spectrum (NuMaximum), the peak of the envelope of oscillation mode ($\nu_{\rm max}$), large frequency separation ($\Delta\nu$) for 561 δ Scuti stars.

TIC Number	Sector	Positions RA	Dec	T_{eff} (K)	Mass ($M/M_{\odot}$)	Radius ($R/R_{\odot}$)	$\log g$	Luminosity $L/L_{\odot}$	Density $\rho/\rho_{\odot}$	TESS mag	ν_f (1/d)	NuMaximum (1/d)	$\nu_{\rm max}$ (1/d)	$\Delta\nu$ (1/d)
81003	11	221.3852	-26.9428	7428 ± 202	1.70 ± 0.29	1.48 ± 0.06	4.33 ± 0.08	6.03 ± 0.54	0.522 ± 0.109	7.79	21.29	21.35	42.42	7.60
148933	11	223.4908	-26.7326	7428 ± 193	1.87 ± 0.30	1.77 ± 0.06	4.22 ± 0.08	10.69 ± 0.83	0.340 ± 0.069	7.79	29.05	45.07	39.49	6.13
589826	5	71.6073	-28.0874	7943 ± 124	1.91 ± 0.30	1.57 ± 0.04	4.33 ± 0.07	8.84 ± 0.16	0.494 ± 0.091	6.02	27.59	48.09	44.84	6.42
975071	8	136.2965	-4.2887	7832 ± 129	1.86 ± 0.29	2.09 ± 0.06	4.07 ± 0.08	14.77 ± 0.53	0.205 ± 0.042	8.56	12.70	22.55	24.02	3.47
1404122	8	140.2844	-16.2399	8721 ± 136	2.19 ± 0.32	1.64 ± 0.05	4.35 ± 0.07	14.08 ± 0.77	0.493 ± 0.089	8.68	47.39	56.51	55.30	7.23
1450658	5	75.1013	-31.8133	7943 ± 128	1.91 ± 0.30	1.46 ± 0.04	4.39 ± 0.08	7.69 ± 0.20	0.608 ± 0.113	7.96	41.89	45.45	48.64	6.83
4351100	6	81.4592	-3.0116	8264 ± 155	2.03 ± 0.30	1.54 ± 0.05	4.37 ± 0.08	9.90 ± 0.70	0.561 ± 0.095	9.98	40.67	52.96	49.08	5.92
5165416	8, 9	142.3168	-38.4035	7492 ± 140	1.72 ± 0.28	1.87 ± 0.07	4.13 ± 0.08	9.98 ± 0.29	0.261 ± 0.056	5.94	12.96	16.85	24.97	4.61
5456605	7	107.8483	-0.3020	7104 ± 134	1.58 ± 0.27	4.08 ± 0.17	3.42 ± 0.09	38.14 ± 1.78	0.023 ± 0.007	5.14	8.25	11.15	10.20	2.05
5586741	7	111.4952	-8.6047	7764 ± 135	1.84 ± 0.29	1.64 ± 0.05	4.27 ± 0.08	8.84 ± 0.34	0.413 ± 0.0774	9.05	40.38	46.83	43.46	6.15
7245720	3	33.1962	-44.4890	7212 ± 136	1.62 ± 0.28	3.16 ± 0.12	3.65 ± 0.09	24.36 ± 1.10	0.051 ± 0.011	7.53	7.92	14.00	13.13	3.03
7808834	4, 5	67.7224	-41.1744	7144 ± 136	1.59 ± 0.27	3.56 ± 0.16	3.54 ± 0.09	29.74 ± 1.34	0.035 ± 0.007	6.49	6.22	6.25	10.80	2.11
9591460	10	193.5049	-25.7537	7517 ± 139	1.74 ± 0.29	1.56 ± 0.05	4.29 ± 0.08	6.98 ± 0.30	0.460 ± 0.089	8.38	19.90	32.83	38.88	6.28
9858459	4	48.4963	-8.8701	7449 ± 105	1.71 ± 0.29	2.10 ± 0.07	4.03 ± 0.08	12.24 ± 0.56	0.184 ± 0.039	9.18	12.64	28.51	25.49	4.73
10838265	3	21.0114	-8.0077	7557 ± 114	1.75 ± 0.28	1.96 ± 0.06	4.10 ± 0.08	11.33 ± 0.33	0.231 ± 0.052	6.00	14.60	30.84	23.59	7.20
10988057	14, 15	303.6338	36.8066	7918 ± 128	1.90 ± 0.31	1.94 ± 0.05	4.14 ± 0.08	13.33 ± 0.34	0.260 ± 0.050	4.79	28.16	37.41	34.91	4.72
11199304	6	84.5453	-1.0503	8670 ± 267	2.17 ± 0.33	1.77 ± 0.06	4.28 ± 0.07	16.01 ± 1.93	0.389 ± 0.070	9.72	38.71	38.70	38.71	6.74
11361473	6	85.1012	-0.7713	9692 ± 733	2.47 ± 0.38	1.51 ± 0.07	4.47 ± 0.09	18.24 ± 4.76	0.711 ± 0.161	10.48	22.46	22.55	48.56	7.51
12524129	4	51.4871	-7.1214	7959 ± 128	1.91 ± 0.30	2.07 ± 0.07	4.09 ± 0.08	15.44 ± 0.69	0.216 ± 0.049	9.05	13.64	27.22	25.06	6.77
12529960	4	51.6614	-9.3663	7377 ± 128	1.68 ± 0.27	1.62 ± 0.06	4.24 ± 0.08	7.03 ± 0.41	0.393 ± 0.079	9.81	18.51	32.40	27.65	5.01
12784216	2	337.3906	-16.8090	7208 ± 122	1.62 ± 0.27	2.34 ± 0.09	3.91 ± 0.09	13.35 ± 0.65	0.126 ± 0.023	8.93	12.30	20.30	26.78	2.28
14773776	22	177.7300	12.2792	7374 ± 128	1.68 ± 0.30	1.62 ± 0.06	4.24 ± 0.09	7.00 ± 0.24	0.395 ± 0.084	6.12	13.63	21.08	26.87	6.20
15833513	20	100.3075	37.1022	8315 ± 164	2.05 ± 0.32	1.70 ± 0.07	4.29 ± 0.08	12.52 ± 1.01	0.414 ± 0.081	9.65	34.79	51.06	46.57	6.57
17466801	24,25	242.7311	32.0030	8314 ± 134	2.05 ± 0.30	1.69 ± 0.05	4.29 ± 0.07	12.33 ± 0.59	0.423 ± 0.075	7.50	46.69	46.66	45.19	6.11
17992601	22	170.9719	37.2348	7518 ± 128	1.74 ± 0.27	3.29 ± 0.11	3.64 ± 0.08	31.19 ± 1.18	0.049 ± 0.010	6.69	10.82	14.77	18.14	2.07
18658256	8,9	137.7702	-34.7247	7373 ± 131	1.68 ± 0.27	1.90 ± 0.07	4.11 ± 0.08	9.63 ± 0.43	0.244 ± 0.049	8.56	15.86	15.90	21.00	6.13
20042408	8	136.9917	-7.8051	6924 ± 131	1.51 ± 0.27	3.55 ± 0.15	3.52 ± 0.09	26.08 ± 1.17	0.034 ± 0.009	7.03	6.38	6.48	14.26	2.32
20296416	5, 6	90.8373	-38.8780	7538 ± 148	1.74 ± 0.28	1.87 ± 0.07	4.14 ± 0.08	10.16 ± 0.44	0.267 ± 0.051	8.82	19.34	29.38	27.04	5.49
20297048	5, 6	90.7633	-37.5470	7774 ± 128	1.84 ± 0.29	1.70 ± 0.05	4.24 ± 0.08	9.49 ± 0.19	0.376 ± 0.071	6.69	17.28	17.28	27.56	5.36
22211065	10	183.3755	-45.1745	7367 ± 133	1.68 ± 0.28	1.62 ± 0.06	4.24 ± 0.08	6.99 ± 0.33	0.393 ± 0.084	8.85	14.69	33.70	29.20	6.25
22234795	9	149.2250	-27.4751	7745 ± 128	1.83 ± 0.29	4.02 ± 0.13	3.49 ± 0.08	52.45 ± 1.95	0.028 ± 0.006	6.14	5.02	17.71	19.79	1.50
22525919	17	2.8986	33.6803	7918 ± 129	1.90 ± 0.30	1.66 ± 0.05	4.28 ± 0.08	9.78 ± 0.32	0.414 ± 0.079	8.51	44.07	44.15	38.28	5.77
22749863	18	38.4222	27.3721	8354 ± 165	2.06 ± 0.31	1.60 ± 0.05	4.35 ± 0.07	11.19 ± 0.70	0.507 ± 0.091	8.84	41.87	41.90	47.17	6.05
23137953	4	46.0564	-8.4645	7412 ± 151	1.69 ± 0.30	2.16 ± 0.08	4.00 ± 0.09	12.70 ± 0.71	0.168 ± 0.033	8.00	12.26	22.90	19.44	3.99
23331223	26	275.1104	31.0357	7422 ± 154	1.70 ± 0.27	1.57 ± 0.05	4.27 ± 0.08	6.78 ± 0.36	0.435 ± 0.088	9.30	21.93	34.39	29.98	7.79
23555158	9, 10	168.9978	-32.3701	7427 ± 138	1.70 ± 0.29	1.71 ± 0.06	4.20 ± 0.08	8.05 ± 0.36	0.338 ± 0.062	8.33	29.83	33.70	33.44	3.71
24344701	5	79.0020	-9.8098	8270 ± 146	2.03 ± 0.30	1.56 ± 0.05	4.36 ± 0.08	10.20 ± 0.64	0.539 ± 0.099	9.74	68.15	72.58	75.17	8.81
24523461	5	80.3114	-7.4800	8290 ± 186	2.04 ± 0.31	1.63 ± 0.05	4.32 ± 0.07	11.31 ± 0.81	0.471 ± 0.098	8.05	35.70	35.42	41.99	4.87
25195864	4-6	63.7537	-69.5367	7523 ± 112	1.74 ± 0.27	3.00 ± 0.12	3.72 ± 0.08	26.04 ± 1.39	0.064 ± 0.016	10.46	5.38	26.78	20.74	3.61
25563502	8 9	144.4729	-30.8806	7747 ± 139	1.83 ± 0.30	2.28 ± 0.07	3.98 ± 0.08	16.87 ± 0.81	0.154 ± 0.041	9.29	11.32	28.51	25.49	5.20
26074369	8	151.0802	-9.1616	7225 ± 139	1.62 ± 0.26	3.06 ± 0.12	3.68 ± 0.08	22.92 ± 1.29	0.057 ± 0.012	8.29	10.26	16.42	13.82	2.60
26174577	8	152.5088	-10.8622	7416 ± 124	1.70 ± 0.29	1.55 ± 0.06	4.29 ± 0.08	6.55 ± 0.29	0.455 ± 0.086	9.13	9.27	23.33	23.67	3.59
26500322	18	57.0771	29.9475	8782 ± 171	2.21 ± 0.32	2.72 ± 0.17	3.91 ± 0.08	39.50 ± 5.45	0.110 ± 0.026	9.08	37.00	39.74	42.42	7.21
26541086	14 15	291.8867	49.2566	7300 ± 144	1.65 ± 0.27	2.12 ± 0.09	4.00 ± 0.08	11.54 ± 0.43	0.172 ± 0.037	7.87	11.77	13.22	21.17	4.71
26633024	24	355.2381	51.3192	8136 ± 137	1.98 ± 0.31	1.63 ± 0.05	4.31 ± 0.08	10.51 ± 0.56	0.456 ± 0.088	10.07	29.94	54.86	48.04	7.05
26749728	14, 15	292.9083	48.4425	8200 ± 145	2.01 ± 0.30	1.60 ± 0.06	4.33 ± 0.08	10.47 ± 0.45	0.487 ± 0.093	8.66	49.90	56.85	54.17	6.55
26957587	21	149.5299	22.6643	7728 ± 127	1.82 ± 0.29	2.03 ± 0.06	4.08 ± 0.08	13.25 ± 0.47	0.217 ± 0.042	8.07	11.33	11.40	29.81	3.40
27420275	16,23	215.6748	38.4818	7393 ± 110	1.69 ± 0.29	2.61 ± 0.09	3.83 ± 0.08	18.38 ± 0.69	0.095 ± 0.020	8.60	8.67	22.55	16.50	4.32
28427365	19	67.6226	46.1500	6191 ± 145	1.19 ± 0.18	3.75 ± 0.29	3.36 ± 0.11	18.66 ± 2.10	0.022 ± 0.007	7.33	8.69	8.73	15.64	1.80
28679106	14	282.8152	33.3234	8094 ± 146	1.97 ± 0.31	1.60 ± 0.05	4.33 ± 0.08	9.84 ± 0.55	0.485 ± 0.094	9.58	41.71	61.17	52.96	6.66

This paper has been typeset from a TEX/LATEX file prepared by the author.